

A minimal statistical-mechanical model for multihyperuniform patterns in avian retina

Enrique Lomba¹, Jean-Jacques Weis³, Leandro Guisández^{1,2}, and Salvatore Torquato^{4,5}

¹*Instituto de Química Física Rocasolano, CSIC, Calle Serrano 119, E-28006 Madrid, Spain*

²*IFLYSIB (UNLP, CONICET), 59 No. 789, B1900BTE La Plata, Argentina*

³*Université de Paris-Saclay, Laboratoire de Physique Théorique, Bâtiment 210, 91405 Orsay Cedex, France*

⁴*Department of Chemistry, Princeton University, Princeton, New Jersey 08544, USA*

⁵*Princeton Institute for the Science and Technology of Materials,
Princeton University, Princeton, New Jersey 08544, USA*

Birds are known for their extremely acute sense of vision. The very peculiar structural distribution of five different types of cones in the retina underlies this exquisite ability to sample light. It was recently found that each cone population as well as their total population display a disordered pattern in which long wave-length density fluctuations vanish [Jiao et al., *Phys. Rev. E*, **84**, 022721 (2014)]. This property, known as hyperuniformity is also present in perfect crystals. In situations like the avian retina in which both the global structure and that of each component display hyperuniformity, the system is said to be multi-hyperuniform. In this work, we aim at devising a minimal statistical-mechanical model that can reproduce the main features of the spatial distribution of photoreceptors in avian retina, namely the presence of disorder, multi-hyperuniformity and local hetero-coordination. This last feature is key to avoid local clustering of the same type of photoreceptors, an undesirable feature for the efficient sampling of light. For this purpose we formulate a simple model that definitively exhibits the required structural properties, namely an equimolar three-component mixture (one component to sample each primary color, red, green, and blue) of non-additive hard disks to which a long-range logarithmic repulsion is added between like particles. A Voronoi analysis of our idealized system of photoreceptors shows that the space-filling Voronoi polygons interestingly display a rather uniform area distribution, symmetrically centered around that of a regular lattice, a structural property also found in human retina. Disordered multi-hyperuniformity offers an alternative to generate photoreceptor patterns with minimal long-range concentration and density fluctuations. This is the key to overcome the difficulties in devising an efficient visual system in which crystal-like order is absent.

I. INTRODUCTION

Sampling light is one of the essential activities that enables the interaction of living organisms with the surrounding environment. From simple devices such as the stigma that provides “vision” in certain classes of microalgae [1], to the sophisticated compound eyes of arthropods [2, 3] living organisms have developed increasingly efficient ways to map visual information from the external world onto signals that can be processed by their cognitive systems. The case of arthropod eyes is particularly interesting. It is known from classical sampling theory [4] that an optimal sampling of light can be achieved by an hexagonal array of photodetectors. This is actually the pattern adopted by ommatidia (the optical units forming a compound eye) in arthropods. Compound eyes are imaging systems with low aberration, wide-angle field of view and infinite field depth[5]. These properties have motivated intense research into the development of bionic compound eyes intended for small robots[6] or sensors for digital cameras[5].

When it comes to vertebrates, with the exception of some teleost fish [7, 8] and some reptiles [8, 9], the situation is different and structural disorder in photoreceptor patterns is the general trend. In this connection, birds are in a class of their own. They possess one of the most elaborate visual systems among vertebrates. In avian retina, one can find five different types of cones, [10, 11], one type for luminance detection and the remaining four

building a tetrachromatic color sensing device covering wavelengths from red to ultraviolet [12]. In contrast with the regular shape of ommatidia in insects, photoreceptors in bird retina are polydisperse, in size and number [13, 14]. This variation provides an adaptative advantage: changing the relative numbers and even pigmentation of the cones bird species can have visual capabilities adapted to different habitats (sea birds have high density of red/yellow cones for hazy conditions, nocturnal birds have a extremely high density of luminance cones, ...). However, polydispersity is known to frustrate crystallization [15], so an alternative to the regular hexagonal pattern of arthropod eyes is needed if we want to preserve a good sampling of light. In this connection, Jiao and coworkers [8] found that the spatial distribution of photoreceptors in chicken retina retained some “hidden order” reminiscent of crystalline patterns. Namely, they found that long-range density and concentration fluctuations were vanishingly small. This feature can be quantified by means of two intimately connected structural properties. In two dimensions, we have first the number variance of cones over a sampling area of radius R , defined as $\sigma_N^2(R) = \langle N^2 \rangle_R - \langle N \rangle_R^2$, where N is the number of cones contained in the sample area and $\langle \dots \rangle_R$ denotes the average over a certain number of sampling areas. In Ref. [8], it was found that this quantity obeys the following large- R asymptotic scaling

$$\sigma_N^2(R) \propto R \quad (1)$$

in the plane. This is one of the possible scalings of hyperuniform systems, also characteristic of crystalline-like order in two dimensions (class I following Ref. [16]). Secondly, it is known that density fluctuations in Fourier space are directly related to the structure factor. This is defined for a set of points/particles with number density ρ by

$$S(\mathbf{Q}) = 1 + \rho \tilde{h}(\mathbf{Q}), \quad (2)$$

where \mathbf{Q} is the wave vector, $\tilde{h}(\mathbf{Q})$ is the spatial Fourier transform of $h(r) = g_2(r) - 1$, being $g_2(r)$ the pair distribution function of the point/particle configuration. It is possible to show [16] that for a system satisfying Eq. (1) in two dimensions then

$$S(Q) \propto Q^\alpha \quad (Q \rightarrow 0) \quad (3)$$

with $\alpha > 0$. Since Eq. (1) holds for each cone distribution, then we will have a relation like (3) for the structure factor computed from each cone pattern, as was found by Jiao and coworkers [8], i.e.

$$\lim_{Q \rightarrow 0} S_{ii}(Q) = 0 \quad (4)$$

for each cone type i . This implies that density fluctuations of the corresponding point patterns will vanish for long wavelengths, i.e. when $Q \rightarrow 0$. The same applies to the overall point pattern. This property was termed in Ref. [8] as “multi-hyperuniformity”.

Interestingly, since Torquato and Stillinger [17] introduced the concept of hyperuniformity and stressed its significance in structurally disordered materials, such exotic “states of matter” have been found in a wide variety of systems. A partial list of examples include amorphous dielectric networks with large and complete photonic band gaps [18, 19], dense transparent disordered media [20], the enhanced pinning of vortices in arrays in superconductors [21], certain composites with desirable transport, dielectric and fracture properties [22–25], sand piles and other avalanche models [26, 27], driven nonequilibrium granular and colloidal systems [28–30] and even immune system receptors [31] all have in common the presence of hyperuniformity.

One might ask why hyperuniformity plays such a crucial role in the quality of vision in birds ?. As mentioned, the optimal sampling configuration of photoreceptors corresponds to a fully regular hexagonal arrangement. Hyperuniformity prevents long-wavelength fluctuations in the photoreceptor density (or concentration of different species) that would be otherwise be present in a structurally disordered configuration of photoreceptors. The presence of such fluctuations is certainly not a desirable property for an accurate image representation. Fully regular arrangements such as the hexagonal patterns of ommatidia are hyperuniform, but in the case of bird retina, crystal-like order is preempted by polydispersity. Thus hyperuniform patterns might well be a good

compromise solution. Multi-hyperuniformity will guarantee the same sampling quality for each type of photoreceptors and aids in ensuring local hetero-coordination, which is key to prevent the unwanted clustering of same color photoreceptors.

After these considerations, it is our aim to build a minimal statistical mechanical model that can reproduce the main characteristics of the photoreceptor distribution. These are, in addition to disorder, on one hand multi-hyperuniformity, and on the other local hetero-coordination. By this we mean that photoreceptors of the same type should not be allowed to cluster together if color sensitivity is to be uniformly distributed on space. In fact, in Ref. [34] it was shown that a system can be multi-hyperuniform and display a strong degree of clustering (chain formation). From pictures of actual chicken cone distributions (see Figure 1 in Ref. [35]) it is readily apparent that cones of different types tend to cluster together, i.e. their spatial distribution displays hetero-coordination.

The findings of Ref. [34] suggest that a mixture with logarithmic long-range repulsions and non-additive hard-core volume exclusions can display the sought characteristics. Strictly speaking the model in question was a two-dimensional Coulomb plasma. Interestingly, in Ref. [8] it was found that the structure factor derived from photoreceptor patterns displays a small wave number decay consistent with $\sim Q$ (or $\sim Q^2$ when fitted into a multiscale packing model [8]). Strictly two-dimensional Coulomb plasmas are known to have structure factors that decay quadratically with the wavenumber as $Q \rightarrow 0$ [36]. Obviously, here the logarithmic repulsion is to be thought of as an effective interaction between photoreceptors. In order to properly account for the presence of hetero-coordination, both the long-range and the short-range hard core repulsions have to be non-additive.

Additionally, we will see that a Voronoi analysis of the disordered hyperuniform patterns further illustrates the hidden connection between these and the fully ordered crystal structures. The area distribution of Voronoi polygons is relatively uniform and centered around that of a crystal like pattern. This uniformity, also found in the Voronoi tessellation of photoreceptors in human retina [44], is in our case the result of the presence of a long-ranged monotonic repulsive interaction.

II. MODEL AND METHODS

As mentioned, our minimal model of “retina” consists of three classes of photoreceptors, (red-green-blue=RGB) in which, following Ref. [34], interactions will be defined in terms of a purely repulsive logarithmic potential. In addition, in order to guarantee hetero-coordination from moderate to high densities, the particles will have a hard-core volume exclusion defined by a hard-disk diameter σ , with unlike particles having a distance of minimum approach $(1 + \Delta)\sigma$, with $\Delta < 0$. From Ref. [34], we know

that $\Delta > 0$ induces the formation of stable clusters of like particles due to the combination of long-range like particle repulsions and an effective short range attraction between like particles due to volume effects. It is worth stressing that our “minimal model” in which for computational simplicity the number of components is reduced to the minimum, three. One can straightforwardly extend the model to four (cyan-magenta-yellow-black=CMYK) or five types (including the luminance cones as in bird retina) of photoreceptors. No significant qualitative difference in the results is to be expected from the consideration of a larger number of photoreceptor types.

The net interaction between particles of type i and j can be explicitly written as

$$\beta u_{ij}(r) = \begin{cases} \infty & \text{if } r < (1 + \Delta(1 - \delta_{ij}))\sigma \\ -\gamma_{ij} \log r/\sigma & \text{if } r \geq (1 + \Delta(1 - \delta_{ij}))\sigma \end{cases} \quad (5)$$

where γ_{ij} is an effective coupling parameter, and δ_{ij} is Kronecker’s symbol. Our minimal model is fully symmetric, with $u_{ii} = u_{11} \forall i$, and $u_{ij} = u_{12} \forall i \neq j$. For the logarithmic repulsion the coupling parameter is expressed as

$$\gamma_{ij} = (\lambda + (1 - \lambda)\delta_{ij})\Gamma \quad (6)$$

with $0 \leq \lambda \leq 1$. The parameter λ controls the non-additivity of the long-range interactions, and we will see it determines whether the system displays multi-hyperuniformity or not.

Now, from our study on binary mixtures in Refs.[34, 37] we know that disordered systems with long-ranged repulsive interactions, whose small wavenumber scaling in Fourier space follows

$$\lim_{Q \rightarrow 0} \beta \tilde{u}_{ij}(Q) \propto Q^{-\alpha} \quad (7)$$

with $\alpha > 0$ will exhibit hyperuniformity. In Ref. [34] we found the conditions that cross interactions must fulfill for a binary system to be multi-hyperuniform. Here we extend our analysis, based on the Ornstein-Zernike (OZ) theory for mixtures, to multi-component systems. A detailed presentation can be found in the Supplementary Information. Our key result, here is that a n -component system in which the small wavenumber behavior of the particle-particle interactions follows (7), will be multi-hyperuniform –i.e. comply with Eq. (4)– if

$$\lim_{Q \rightarrow 0} |\tilde{\mathbf{u}}(Q)| \neq 0 \quad (8)$$

where $|\dots|$ denotes a matrix determinant, and the elements of the matrix $\tilde{\mathbf{u}}(Q)$ are the Fourier transform of the species-species interactions, $u_{ij}(r)$. It can be shown that a sufficient condition for Eq. (8) to be fulfilled is that

$$\lim_{Q \rightarrow 0} [\tilde{u}_{ii}(Q)\tilde{u}_{jj}(Q) - \tilde{u}_{ij}(Q)^2] \neq 0, \quad (9)$$

which actually means that cross interactions must **not** comply with the Lorentz-Berthelot mixing rules in the long wavelength limit. This we had already found for binary mixtures in Ref. [34]. In practice, for our model system this means that $\lambda < 1$. Here we will simply set $\lambda = 0$ which reduces cross interactions to bare hard-core repulsions.

The low- Q asymptotics of the structure factor when all densities are identical ($\rho_i = \rho/3 \forall i$) simplifies considerably. A detailed derivation can be found in the supplementary information based on the low- Q expansion of the OZ equation. In our particular case, given the symmetry of the interactions and compositions and setting $\lambda = 0$, from Eq. (S.11) in the SI the limiting behavior of the partial structure factors reduces to

$$\begin{aligned} \lim_{Q \rightarrow 0} S_{ii}(Q) &= Q^2/(2\pi\rho\Gamma), \quad \forall i \\ \lim_{Q \rightarrow 0} S_{ij}(Q) &= \rho\tilde{c}_{ij}^R(0)Q^4/(2\pi\rho\Gamma)^2, \quad \forall i \neq j. \end{aligned} \quad (10)$$

with $\tilde{c}_{ij}^R(Q)$ being the Fourier transform of the short range component of the direct correlation function (cf SI for further details), which is non-zero and finite as $Q \rightarrow 0$. When considering mixtures, it is important to monitor the global hyperuniformity using the the number-number structure factor. This is simply the net structure factor given by Eq. (2) where the pair distribution function is computed using all particle types. In practice it can be also computed from the addition of the partial structure factors as

$$S_{NN}(Q) = \sum_{i,j} S_{ij}(Q). \quad (11)$$

From Eq. (10) we then have

$$\lim_{Q \rightarrow 0} S_{NN}(Q) = 3Q^2/(2\pi\rho\Gamma) + bQ^4. \quad (12)$$

where $b = 3\rho\tilde{c}_{ij}^R(0)/(2\pi\rho\Gamma)^2$.

The systems studied in this work have been analyzed using an integral equation approach based on the OZ equation, Eq. (S.1), with a Reference Hypernetted Chain (RHNC) closure (Eq. (11) in Ref. [37]). We refer the reader to [37] for further details on the numerical approach to solve this equation. We have also performed extensive canonical (NvT) Monte Carlo simulations, in which the energy of the periodic system is evaluated using the Ewald technique with conducting boundary conditions[37, 38]. Computational details of the simulations are identical to those of Ref. [37].

III. RESULTS

We will first consider two instances of photoreceptor patterns for low density ($\rho\sigma^2 = 0.2$), and moderate density ($\rho\sigma^2 = 0.8$), with an interspecies hard core exclusion defined by $\Delta = -0.2$ (i.e. $\sigma_{ij} = 0.8\sigma_{ii}$). The coupling factor of the long range interaction is set to $\Gamma = 5$,

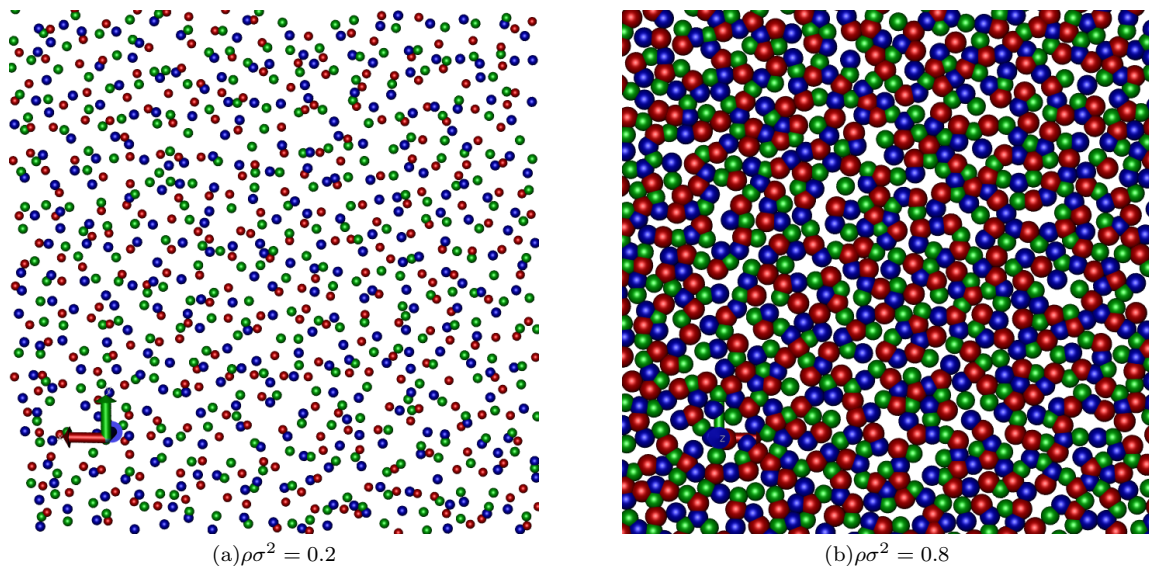


FIG. 1. Snapshots of Monte Carlo configurations of our three component minimal model of retina with *rgb* receptors (as shown in the Figure). The interaction is defined by a coupling $\gamma = 5$ and a non-additivity parameter $\Delta = -2$.

and the long-range cross interactions are set to zero (i.e. $\lambda = 0$ in (5)). This means that unlike particles will only interact via a pure hard core exclusion. For comparison we will also show results for $\lambda = 1$ which will only display global hyperuniformity. Partial densities for each photoreceptor type are $\rho\sigma^2/3$.

Two characteristic Monte Carlo snapshots of the low and high density multihyperuniform systems are presented in Figure 1. One can appreciate in the snapshot of 1(a) for $\rho\sigma^2 = 0.2$ that photoreceptors of different type tend to aggregate in clusters with hetero-coordination. These clusters form a low density fluid-like structure, with average inter-cluster distances $\approx 3-4\sigma$. When comparing this illustration with real representations of bird cone distributions (see Figure 1 in Ref. [35]) the similarity is evident. At higher densities ($\rho\sigma^2 = 0.8$) packing effects become dominant and clustering is not so apparent, but hetero-coordination is still clearly seen in the snapshot of Figure 1(b). The cluster size distribution (not shown) is monotonously decreasing, with no dominant cluster size. This is a consequence of the lack of a competing short range attraction that would counteract the long-range repulsion and would thus stabilize finite size clusters, as it was the case for $\Delta > 0$ in Ref. [34].

A. Structure factor analysis

In Figure 2 we plot the partial and total structure factors corresponding to the systems described above. The multi-hyperuniform character of the system is clearly illustrated by their vanishing behavior for low- Q . In the insets one can observe that they closely follow the asymptotic behavior described by Eqs. (10) and (12). Theory

and simulation agree to a very large extent.

For comparison we also plot the theoretical results for $\rho\sigma^2 = 0.2$, and $\lambda = 1$. Now, this choice of the long-range cross interactions leads to a globally hyperuniform configuration, as confirmed by the behavior of $S_{NN}(Q)$ as $Q \rightarrow 0$. In contrast, the partial structure factor does not vanish for $Q \rightarrow 0$ (which rules out multihyperuniformity). Given the low density, the result is close to that of an ideal gas, for which $S_{ii}(Q) \approx x_i \forall Q$. Reducing λ , which actually implies decreasing (or in our present case, eliminate) the unlike long-range repulsive interactions, induces a certain degree of clustering between unlike particles. This effect is visible when comparing the total structure factor at low density (lower graph, red curve in Figure 2) for $\lambda = 0$ and $\lambda = 1$. Only in the case of $\lambda = 0$, $S_{\alpha\alpha}(Q)$ exhibits a prepeak at $Q\sigma \approx 1.9$. This reflects the presence of clustering with a correlation length of $\approx 3.2\sigma$ which we have already qualitatively detected in the snapshot of Figure 1(a). In summary, the combination of very long-ranged repulsions between like particles with non-additive unlike interactions both in the short and long range reproduces the features sought for in our minimal statistical mechanical model of retina.

B. Mimicking avian retina

How do our model results compare with a real structure factor obtained from a distribution of avian photoreceptors? One must first bear in mind that in bird retina five different types of photoreceptors [8] are present in unequal numbers, so in principle our model departs significantly from the real situation. Nonetheless, a simple inspection of the experimental structure factors pre-

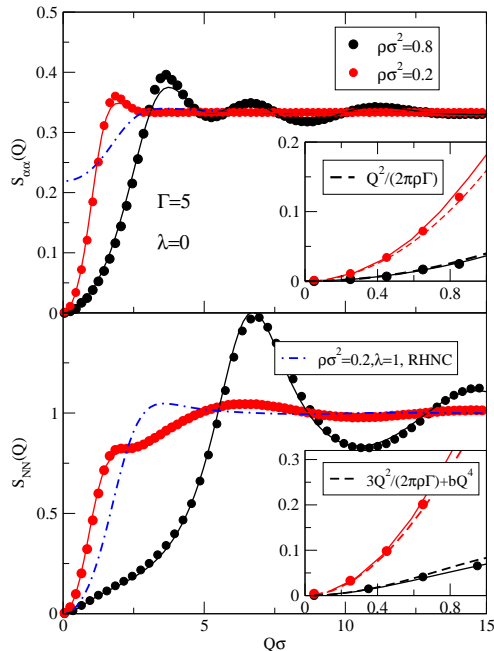


FIG. 2. Total and partial structure factors of our model photoreceptor system displaying multi-hyperuniformity for low and moderate number densities (see legend). Solid and dash-dotted curves correspond to theoretical (RHNC) calculations, symbols denote Monte Carlo data. Dashed curves in the insets represent the low- Q regime derived from Eq.(10). Partial structure factors correspond to correlations between like particles. For comparison we show on blue dash-dotted curves the structure factors for a system displaying only global hyperuniformity ($\lambda = 1$ in Eq. (5)).

presented in Figure 9 of Ref. [8] indicates that basically all photoreceptor species qualitatively display similar partial structure factors. The global structure factor is qualitatively different, with very little structure at low Q values. Therefore, it seems reasonable to compare our model system with actual experimental results from a qualitative standpoint. To that aim, we have adjusted the coupling constant Γ of our effective potential to match the results of [8]. Density is basically coupled to Γ (except for subtle hard core effects not visible in the low Q behavior of the structure factor), so we have set $\rho\sigma^2 = 0.8$ and kept it fixed. As in Ref. [8] Q is scaled with the position of the structure factor maximum, which sets the length scale to the appropriate value in order to ease the comparison. This is equivalent to rescaling the data so as to account for the appropriate sizes of the photoreceptors. We observe that the behavior of our simple model depicted in Figure 3 agrees qualitatively with the experimental data. As a matter of fact, even if in Ref. [8] the experimental low- Q behavior seems to follow a linear decay instead of

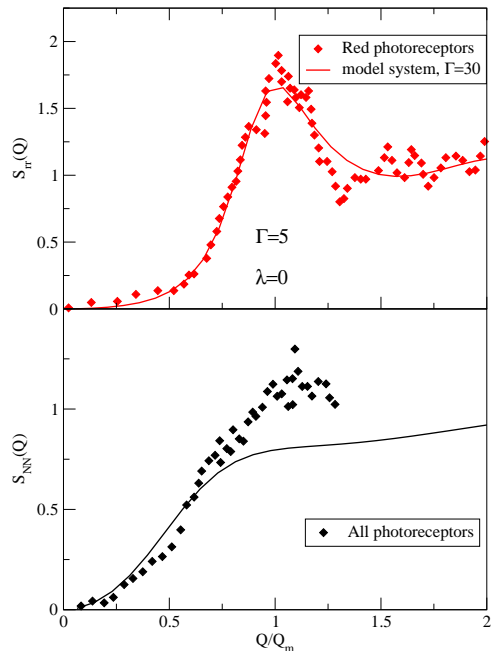


FIG. 3. Total and partial structure factor of the symmetric three component plasma with negative non-additivity for $\lambda = 0$, $\rho\sigma^2 = 0.8$, $\Gamma = 30$ compared with those from avian photoreceptors from Ref. [8]. In the upper curve only the red photoreceptors are presented. Solid curves correspond to RHNC calculations, symbols to experimental data[8]. The partial structure factor is normalized to one and the Q axis is scaled with the position of the maximum which is equivalent to adjust σ to the effective experimental value in the photoreceptor correlations.

the Q^2 dependence of our model, the quadratic dependence appears acceptable. Interestingly, the multiscale packing model also proposed by Jiao and coworkers[8] displays the same quadratic decay. The other salient feature that is observed in Figure 3 is the lack of structure of $S_{NN}(Q)$ for low Q values. This feature is visible both in our simple model (although somewhat enhanced) and in the experimental data. It is apparent that our minimal model is capable of reproducing key features of the spatial patterns display by photoreceptors in actual bird retina.

C. Voronoi analysis

When thinking of photoreceptors, one must also take into account that their ability to reproduce an image is directly related with the area they sample. This suggests that a Voronoi analysis of our point configurations will provide information as to the sampling area correspond-

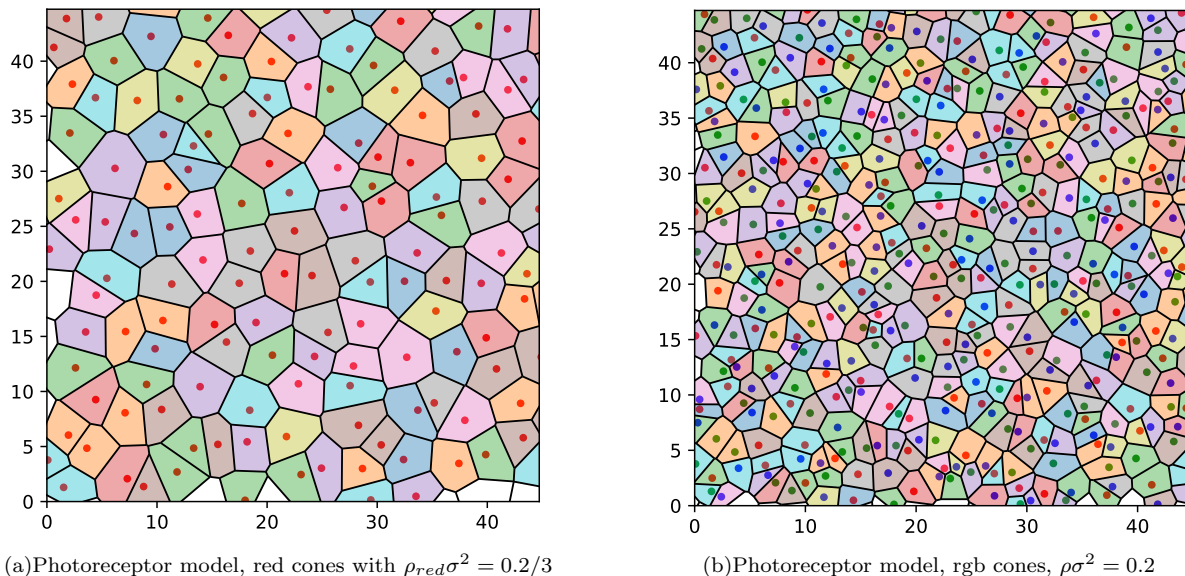


FIG. 4. Voronoi tessellations corresponding to the red cones (left) of the photoreceptor model and all the photoreceptors (right) for total density $\rho\sigma^2 = 0.2$.

ing to each particle. We have therefore performed a characterization of the spatial configurations of our model system using Voronoi tessellations. We have studied the corresponding area distribution of the Voronoi polygons. In order to put these results in perspective, we have also performed a corresponding analysis for purely random two-dimensional point configurations, as well as configurations obtained from Molecular Dynamics simulations for 2D fluids of Lennard-Jones (LJ) particles and LJ particles with added Coulomb repulsion. In the last instance, the competition between short-range attractive and long-range repulsive forces leads to the formation of stable clusters that nonetheless display hyperuniformity. For these cases, we have used similar density conditions and supercritical temperatures ($k_B T/\epsilon = 2.0$, where k_B is Boltzmann's constant and T the absolute temperature). When referring to LJ results, ϵ and σ correspond to the well depth and particle size respectively. These results are presented in detail in the Supplementary Information. Upon examination of Figure 4, one can clearly appreciate that in our model system the Voronoi tessellation exhibits a fairly regular distribution of the polygon areas. A similar observation was made by Legras et al. [44] when analyzing the cone distribution in human retina. However, when comparing with tessellations for LJ fluids or random distributions (see Figure 1 of the SI) at similar density, one finds that these have a much larger dispersion in their areas. This can be more quantitatively analyzed by examining the normalized area distributions. These are plotted in Figure 5 vs the area scaled with the corresponding particle densities, ρA . The corresponding figure for random and LJ can be found in the SI.

Figure 5 reveals that our model leads to the area distributions that are symmetrized with respect to the regular

lattice result, $\rho A = 1$. It is interesting to note that in all cases the curves apparently follow a Gaussian distribution. In contrast, area distributions for random configurations and LJ particles at low density follow highly asymmetric Γ -distributions, and denser packings of LJ particles can be fit to log-normal distributions (see SI). It is important to note that the symmetrization of the area distributions is not a consequence of hyperuniformity. In Ref. [33], it was found that certain stealthy hyperuniform patterns led to asymmetric distributions similar to those of random configurations. This is also illustrated by the analysis of LJ particles with added Coulombic repulsions, which form hyperuniform patterns with a strong degree of clustering. The area distribution of the Voronoi polygons is a short/medium range property, unlike hyperuniformity which is a large-scale property.

For our retina model, the marked symmetry of the Voronoi area distribution is due to the fact that the interactions are monotonic and repulsive, and thus tend to produce very regular local environments. This is illustrated by the uniform linear behavior of number variance $\sigma_N^2(R)$ for both the global and the single species photoreceptor configurations in our model, as can be seen in Figure 6. The same linear dependence is found in the experimental photoreceptor distributions (see Figure 4 in Ref. [8]). Conversely, hyperuniform configurations that display clustering (and asymmetric area distributions of their Voronoi tessellations) present a number variance with a clear non-monotonic behavior for small sampling windows. Such is the case of particles with LJ+Coulombic interactions as illustrated in Fig. 3 of the SI.

One can then interpret the symmetrization of the area distribution in a disordered media as the con-

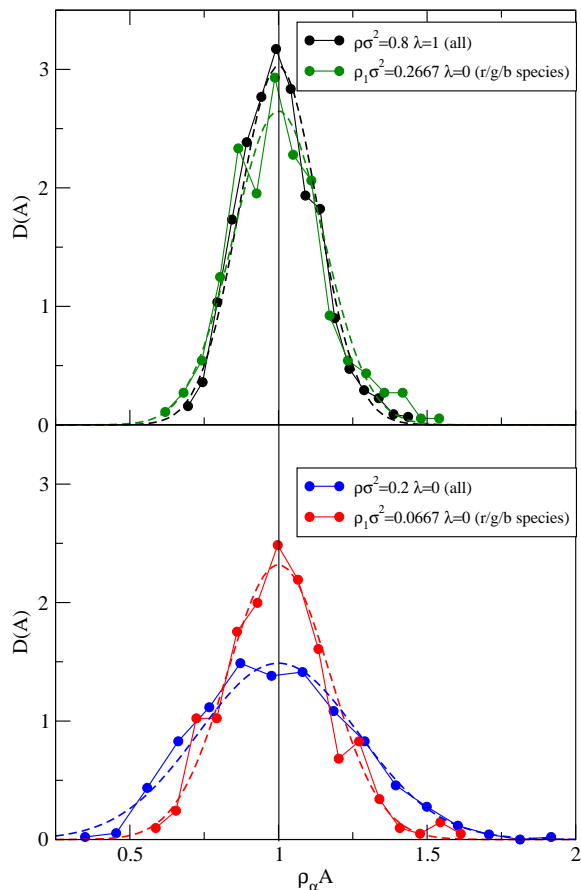


FIG. 5. Scaled area distribution of the Voronoi polygons for hyperuniform states: high density (upper graph) and low density (lower graph) single species and global configurations of the three-component plasma. Hyperuniformity symmetrizes the area distributions around the value of the square regular lattice ($\delta(\rho A - 1)$) and the curves follow an apparent Gaussian distribution (as shown by the fits represented by dashed curves).

sequence of the minimization of repulsive interactions, maximizing the area around each point in the configuration, and reflecting random deviations from the crystalline (ordered hyperuniform) state. This, together with the strong suppression of long-wavelength density and concentration fluctuations leads to what could possibly be optimal photoreceptor patterns.

IV. CONCLUDING REMARKS

In summary, we have shown that two key features of the experimental patterns of photoreceptors in bird retina, multi-hyperuniformity and hetero-coordination, can be captured by a simple model with logarithmic repulsions between like particles and hard core exclusions with negative non-additivity between the unlike ones. The fact that disordered hyperuniform systems represent

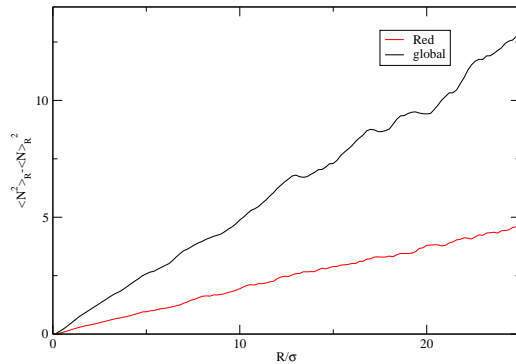


FIG. 6. Number variance $\sigma_N^2(R)$ dependence of sample window radius, R , for both the global and the single species photoreceptor model configurations.

topological states of matter sharing fluid and crystal-like properties makes them the solution of choice when regular arrangements such as those of arthropod eyes are hampered by the variability of the photoreceptors (e.g. unequal sizes and numbers). Present day bio-inspired optical devices rely on regular arrangements [5, 41]. In certain instances, the combination of different types of receptors and in different number might be required compromising the feasibility of regular arrays of receptors. Disordered multi-hyperuniformity might then offer an alternative to overcome these difficulties.

A natural extension of this work should be the extension to non-Euclidean geometries. Steps in this direction can be found in the works of Meyra et al. [42] and Božič and Čopar [43] for spherical surfaces. Actually designs on curved surfaces have been already proposed for regular arrays in Ref. [5]. Disorder hyperuniform systems on curved surfaces might well have a potentially larger impact on technological applications. An analysis along these lines of photoreceptor patterns in humans [44] might also be of interest to further our understanding of our complex visual system. In fact, in Ref. [44] it was found that human cones tend to preserve locally hexagonal arrangements. A preliminary Voronoi analysis of the area distributions taken from Ref. [44] show that these are also relatively symmetric. On the other hand, photoreceptor patterns in human retina are also dependent on the eccentricity of the sampling area, and this considerably complicates the analysis.

ACKNOWLEDGMENTS

EL acknowledges the support from the Agencia Estatal de Investigación and Fondo Europeo de Desarrollo Regional (FEDER) under grant No. FIS2017-89361-C3-2-P. EL and LG were also supported by the European

Union's Horizon 2020 Research and Innovation Staff Exchange programme under the Marie Skłodowska-Curie grant agreement No 734276. S.T. was supported by the

National Science Foundation under Award No. DMR-1714722. The authors are grateful to Prof. Y. Yiao for kindly providing the structure factor data from Ref. [8].

-
- [1] P. Hegemann, *Planta* **203**, 265 (1997).
- [2] D. F. Ready, T. E. Hanson, and S. Benzer, *Dev. Biol.* **53**, 217 (1976).
- [3] D. K. Lubensky, M. W. Pennington, B. I. Shraiman, and N. E. Baker, *Proc. Natl. Acad. Sci. U.S.A.* **108**, 11145 (2011).
- [4] D. P. Petersen and D. Middleton, *Inf. Control* **5**, 279 (1962).
- [5] Y. M. Song, Y. Xie, V. Malyarchuk, J. Xiao, I. Jung, K.-J. Choi, Z. Liu, H. Park, C. Lu, R.-H. Kim, R. Li, K. B. Crozier, Y. Huang, and J. A. Rogers, *Nature* **497**, 95 (2013).
- [6] Y. Zheng, L. Song, J. Huang, H. Zhang, and F. Fang, *Optics Letters* **44**, 4143 (2019).
- [7] P. A. Raymond and L. K. Barthel, *Int. J. Dev. Biol.* **48**, 935 (2004).
- [8] Y. Jiao, T. Lau, H. Hatzikirou, M. Meyer-Hermann, J. C. Corbo, and S. Torquato, *Phys. Rev. E* **89**, 022721 (2014).
- [9] R. F. Dunn, *J. Ultrastruct. Res.* **16**, 672 (1966).
- [10] M. Ruggeri, J. C. Major, C. McKeown, R. W. Knighton, C. A. Puliafito, and S. Jiao, *Invest. Ophthalmol. Vis. Sci.* **51**, 5789 (2010).
- [11] M. B. Toomey and J. C. Corbo, *Front. Neural Circuit.* **11**, 97 (2017).
- [12] J. Withgott, *BioScience* **50**, 854 (2000).
- [13] T. H. Goldsmith, J. S. Collins, and S. Licht, *Vision Res.* **24**, 1661 (1984).
- [14] B. A. Moore, P. Baumhardt, M. Doppler, J. Randollet, B. F. Blackwell, T. L. DeVault, E. R. Loew, and E. Fernandez-Juricic, *J. Exp. Biol.* **215**, 3442 (2012).
- [15] D. Frenkel, "Introduction to colloidal systems," (Taylor and Francis, 2006).
- [16] S. Torquato, *J. Phys. : Condens. Matter* **28**, 414012 (2016).
- [17] S. Torquato and F. H. Stillinger, *Phys. Rev. E* **68**, 041113 (2003).
- [18] M. Florescu, S. Torquato, and P. J. Steinhardt, *Proc. Natl. Acad. Sci. U.S.A.* **106**, 20658 (2009).
- [19] L. S. Froufe-Pérez, M. Engel, J. J. Sáenz, and F. Scheffold, *Proc. Natl. Acad. Sci. U.S.A.* **114**, 9570 (2017).
- [20] O. Leseur, R. Pierrat, and R. Carminati, *Optica* **3**, 763 (2016).
- [21] Q. Le Thien, D. McDermott, C. J. O. Reichhardt, and C. Reichhardt, *Phys. Rev. B* **96**, 094516 (2017).
- [22] G. Zhang, F. H. Stillinger, and S. Torquato, *J. Chem. Phys.* **145**, 244109 (2016).
- [23] D. Chen and S. Torquato, *Acta Mater.* **142**, 152 (2018).
- [24] Y. Xu, S. Chen, P.-E. Chen, W. Xu, and Y. Jiao, *Phys. Rev. E* **96**, 043301 (2017).
- [25] B.-Y. Wu, X.-Q. Sheng, and Y. Hao, *PloS one* **12**, e0185921 (2017).
- [26] R. Dickman and S. D. da Cunha, *Phys. Rev. E* **92**, 020104R (2015).
- [27] R. Garcia-Millan, G. Pruessner, L. Pickering, and K. Christensen, *Europhys. Lett.* **122**, 50003 (2018).
- [28] D. Hexner and D. Levine, *Phys. Rev. Lett.* **114**, 110602 (2015).
- [29] J. H. Weijs, R. Jeanneret, R. Dreyfus, and D. Bartolo, *Phys. Rev. Lett.* **115**, 108301 (2015).
- [30] E. Tjhung and L. Berthier, *Phys. Rev. Lett.* **114**, 148301 (2015).
- [31] A. Mayer, V. Balasubramanian, T. Mora, and A. M. Walczak, *Proc. Nat. Acad. Sci.* **112**, 5950 (2015).
- [32] O. U. Uche, F. H. Stillinger, and S. Torquato, *Phys. Rev. E* **70**, 046122 (2004).
- [33] G. Zhang, F. H. Stillinger, and S. Torquato, *Phys. Rev. E* **92**, 022119 (2015).
- [34] E. Lomba, J.-J. Weis, and S. Torquato, *Phys. Rev. E* **97**, 010102(R) (2018).
- [35] Y. A. Kram, S. Mantey, and J. C. Corbo, *PLoS ONE* **5**, e8992 (2010).
- [36] J. M. Caillol, D. Levesque, J. J. Weis, and J. P. Hansen, *J. Stat. Phys.* **28**, 325 (1982).
- [37] E. Lomba, J. J. Weis, and S. Torquato, *Phys. Rev. E* **96**, 062126 (2017).
- [38] S. Leeuw and J.W.Perram, *Physica A* **113**, 546 (1982).
- [39] M. Ferraro and L. Zaninetti, *Physica A: Statistical Mechanics and its Applications* **391**, 4575 (2012).
- [40] M. A. Klatt, J. Lovrić, D. Chen, S. C. Kapfer, F. M. Schaller, P. W. A. Schönhöfer, B. S. Gardiner, A.-S. Smith, G. E. Schröder-Turk, and S. Torquato, *Nature Comm.* **10**, 811 (2019).
- [41] M. Garcia, C. Edmiston, T. York, R. Marinov, S. Mondal, N. Zhu, G. P. Sudlow, W. J. Akers, J. Margenthaler, S. Achilefu, R. Liang, M. A. Zayed, M. Y. Pepino, and V. Gruev, *Optica* **5**, 413 (2018).
- [42] A. G. Meyra, G. J. Zarragoicoechea, A. L. Maltz, E. Lomba, and S. Torquato, *Phys. Rev. E* **100**, 022104(R) (2019).
- [43] A. L. Božič and S. Čopar, *Phys. Rev. E* **99**, 032601 (2019).
- [44] R. Legras, A. Gaudric, and K. Woog, *PLOS ONE* **13**, e0191141 (2018).